An algorithm for calculating the Lorentz angle in silicon detectors

V. Bartsch [a] W. de Boer [a] J. Bol [a] A. Dierlamm [a] E. Grigoriev [a] F. Hauler [a] S. Heising [a,b] L. Jungermann [a]

[a] *Institut für Experimentelle Kernphysik, Universität Karlsruhe (TH), P.O. Box 6980, 76128 Karlsruhe, Germany*

[b] *European Laboratory for Particle Physics (CERN), CH-1211 Geneve 23, Switzerland*

Abstract

The CMS (Compact Muon Solenoid) detector will use silicon sensors in the harsh radiation environment of the LHC (Large Hadron Collider) and high magnetic fields. The drift direction of the charge carriers is affected by the Lorentz force due to the high magnetic field. Also the resulting radiation damage changes the properties of the drift. The CMS silicon strip detector is read out on the p-side of the sensors, where holes are collected, while the pixel sensors have n-side read out, thus collecting electrons.

In this paper measurements of the Lorentz angle are reviewed. Easy algorithms to compute the Lorentz angle are proposed.

Key words: silicon, sensors, detectors, Lorentz angle, magnetic field, CMS

1 Introduction

The Lorentz angle Θ_{L}, by which charge carriers are deflected in a magnetic field perpendicular to the electric field (see Fig. 1), is defined by:

$$\tan(\Theta_{\mathrm{L}}) = \frac{\Delta x}{d} = \mu_{\mathrm{H}} B = r_{\mathrm{H}} \mu B \tag{1}$$

where d corresponds to the drift distance along the electric field and Δx to the shift of the signal position. If the ionization is only produced at the surface the drift distance equals the detector thickness. If the ionization is produced homogeneously by a traversing particle, the averaged drift distance is only half

the detector thickness. The Hall mobility is denoted by μ_{H}, the conduction mobility by μ. The Hall mobility differs from the conduction mobility by the Hall scattering factor r_{H}. This factor describes the influence of the magnetic field on the mean free path of carriers of different energy (2). The Hall scattering factor has a value of ≈ 0.7 for holes and ≈ 1.15 for electrons at room temperature. The mobility μ increases with temperature proportional to $T^{-2.5}$ for holes and $T^{-2.2}$ for electrons (3). The hole mobility is about $470\,\mathrm{cm}^2/\mathrm{Vs}$ at 300 K, the electron mobility is about $1417\,\mathrm{cm}^2/\mathrm{Vs}$ at 300 K, thus the drift mobility of electrons is about three times larger than the hole mobility. Therefore the Lorentz shift is considerably larger for electrons than for holes. Thus p-side read out shows a considerably smaller Lorentz shift than n-side read out. Still the Lorentz shifts for holes generated at the surface reach about $40\,\mu$m ($70\,\mu$m) in a 4 T magnetic field for a $320\,\mu$m ($500\,\mu$m) thick detector, so that the shifts should be accounted for.

As can be seen on the right hand side of Fig. 1 it is clear that a minimum ionising particle (MIP) gives a broader signal for electrons (n-side) than for holes (p-side), as sketched in Fig. 2.

Another important question is the dependence of the Lorentz shift on the irradiation dose. The change of drift mobility and electric field in the silicon detector due to defects introduced by radiation damage results in a change of the Lorentz shift and thus of the calibration of the detector.

2 Special properties of the silicon strip detectors of CMS

The silicon tracker of CMS (5) can be divided into an inner tracker, which consists of an inner barrel and an inner endcap, and an outer tracker, which consists of an outer barrel and an outer endcap. The sensors for the inner tracker will have a bulk resistivity of ρ = 1.5-3 kΩcm and a thickness of $d = 320\,\mu$m whereas the outer tracker will have a bulk resistivity of ρ = 3.5 - 6 kΩcm and a thickness of $d = 500\,\mu$m (4). The $500\,\mu$m thick sensors have strip pitches between 122 and $205\,\mu$m, the $320\,\mu$m thick sensors have strip pitches between 80 and $158\,\mu$m. The whole silicon tracker is situated in a magnetic field of 4 T. The maximum fluences, to which the silicon strip sensors of CMS are exposed, reach fluences equivalent to about $2{\cdot}10^{14}\,1\,\mathrm{MeV\,n/cm}^2$ at the expected luminosity of $5{\cdot}10^5\,\mathrm{pb}^{-1}$. The distribution of the fluences over the silicon tracker is shown in Fig. 3.

This harsh radiation environment implies that the properties of the silicon sensors will change and this affects the Lorentz angle as discussed previously (6). The expected maximum full depletion voltage for the highest fluence level reaches $\approx$350 V (7; 8). So the silicon strip sensors will still run at full depletion,

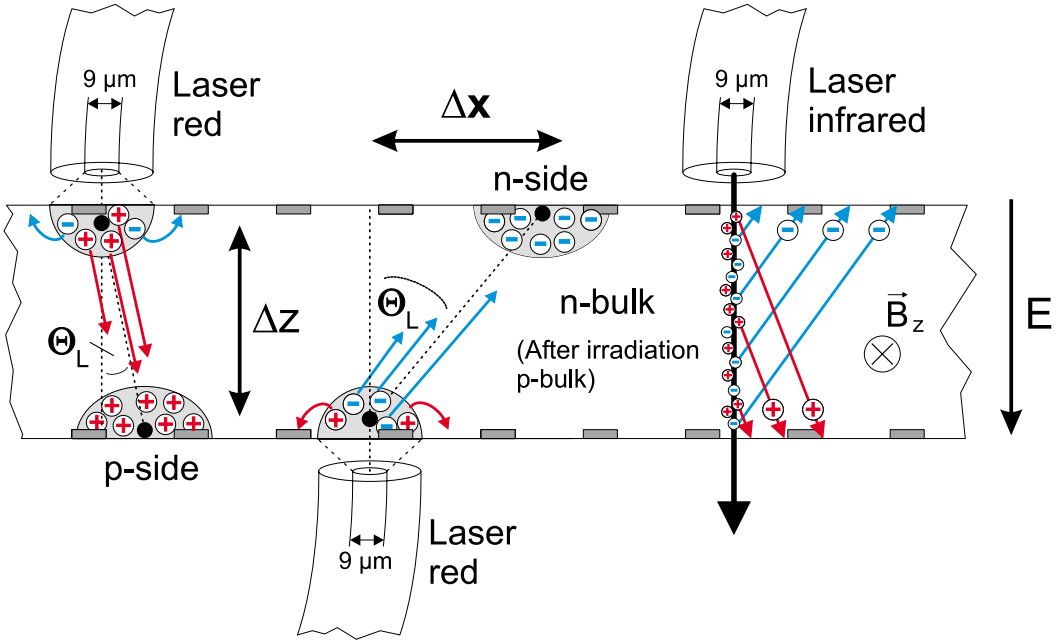

Fig. 1. *The figure shows the principle of the Karlsruhe setup to measure the Lorentz angle of holes and electrons (1). It is equipped with three fibers delivering laser light to the silicon. The red lasers have a penetration depth of a few µm, so with a laser pulse on the n-side or p-side one can measure the drift of electrons and holes, respectively. The infrared laser generates charge throughout the whole thickness of the detector.*

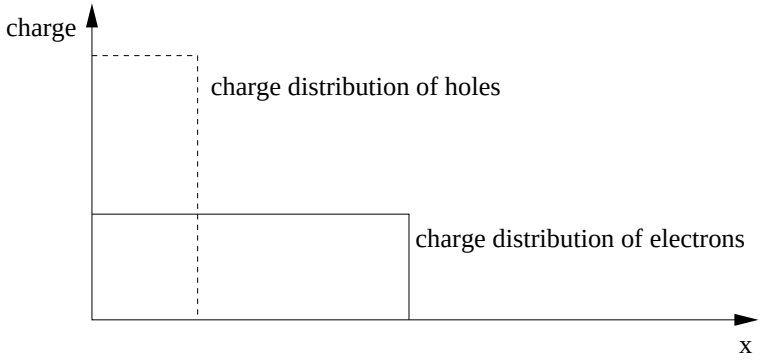

Fig. 2. *Distribution of charge from a MIP on p- and n-side in a simple model (no segmentation of the contacts and no diffusion included).*

since the breakdown voltage is specified to be at least 500 V.

3 Experimental results

Experimental studies of the Lorentz shift in non-irradiated and irradiated silicon sensors are the basis of the algorithms used for the silicon strip detector in CMS. A comprehensive study of Lorentz shifts of non-irradiated and irra-

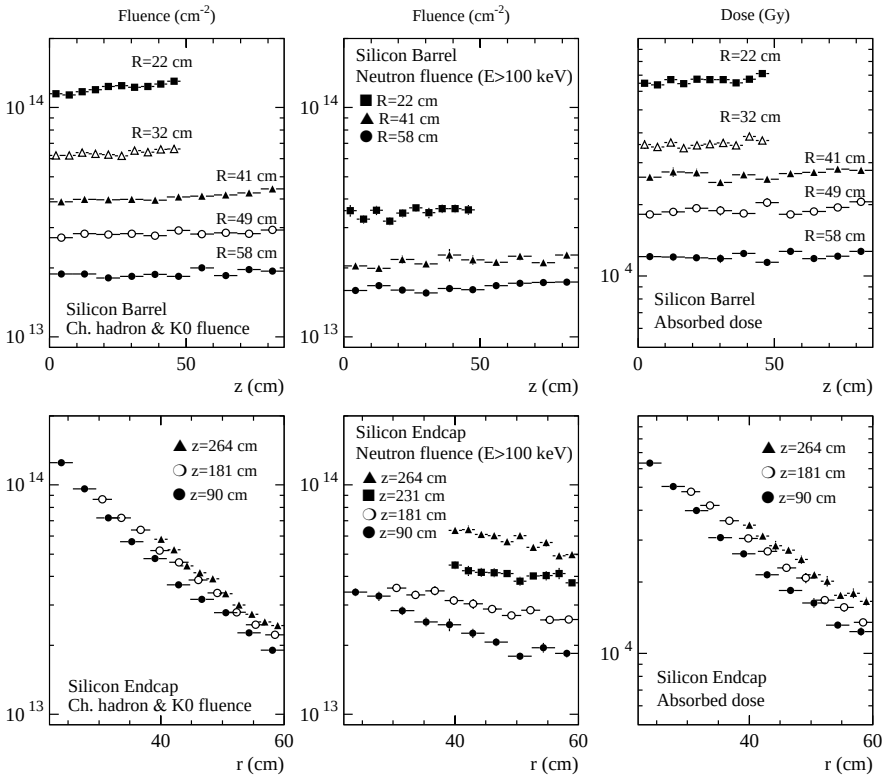

Fig. 3. *Energy-integrated charged hadron and neutron fluences and absorbed doses in the silicon tracker. All values are for an integrated luminosity of* $5 \cdot 10^5\ pb^{-1}$. *(5)*

diated sensors was performed at Karlsruhe (1; 9; 10; 11). The Lorentz angle has been measured for electrons and holes separately. A temperature range of 77 K-300 K was covered. The Lorentz angle is measured by injecting charges at the surface on one side and observing the drift through the sensor by measuring the position of the charge on the opposite side (see Fig. 1). Alternative methods are described in (12; 13).

Charges are generated by injecting laser light with a wavelength of $\lambda \approx 650\,\mathrm{nm}$, which has an absorption length of $\approx 3\,\mu$m at 300 K. Using the red laser charge carriers of one type are collected at the nearest electrode, whereas the carriers of the other type drift towards the opposite side. This allows the measurement of the Lorentz angle for electrons and holes separately by injecting laser light either on the p- or n-side. To simulate a MIP an infrared laser with a wavelength of 1060 nm was used, which has an absorption length of $\approx 300\,\mu$m at room temperature.

For the measurements the JUMBO magnet from the Forschungszentrum Karlsruhe (14) was used in a $B \leq 10\,\mathrm{T}$ configuration with a warm bore of 72 mm. The sensors are double sided "baby" detectors of approximately 2x1 cm from the HERA-B production by Sintef. They have a strip pitch of 50 μm on the

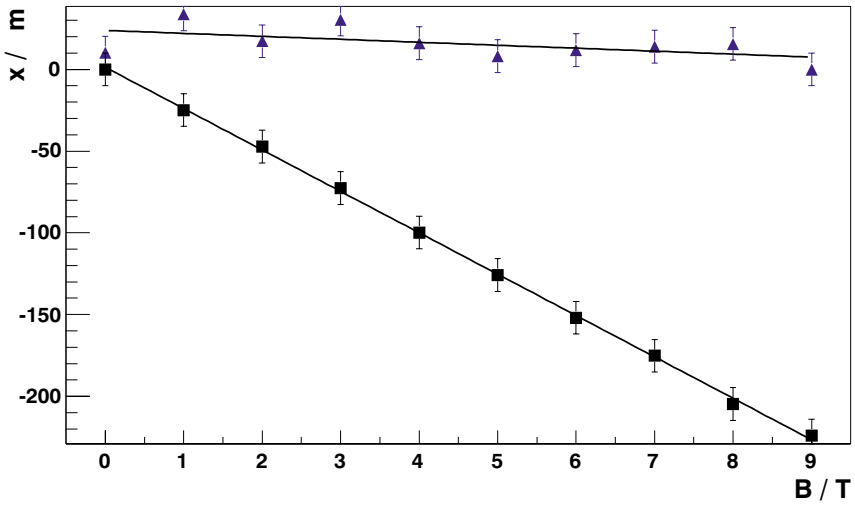

Fig. 4. *The Lorentz shift of electrons (top curve) and holes (lower curve) versus magnetic field. The red laser (≈ 650 nm) pulse on the n-side side hardly penetrates, so the electrons are immediately collected by the neighbouring strips on the n-side and the holes drift through the sensor to the p-side. Therefore a significant shift is seen only for the holes. The temperature is 166K, the bias voltage 150 V.*

p–side and 80 μm on the n–side; the strips on opposite sides are oriented at an angle of 90° with respect to each other. The signal position is computed using either a fit with the sum of two Gaussians or the center of gravity:

$$\bar{x}(PH) = \frac{\sum PH_{\mathrm{i}} x_{\mathrm{i}}}{\sum PH_{\mathrm{i}}}. \tag{2}$$

Here PH_{i} is the pulse height of the strip i and x_{i} its position.

The signal position is plotted as function of the magnetic field in Fig. 4, which shows clearly that the Lorentz shift is linear with the magnetic field up to 9 T. This implies that Eq. 1 can be used at the 4 T magnetic field of CMS.

Before irradiation the detector depletes fully at a bias voltage of 40 V, while after irradiation with $1.0{\cdot}10^{13}$ 21 MeV protons / cm^2 the depletion voltage has increased to 100 V. This implies that the bulk is inverted from n-type to p-type material, as expected (15). The bulk damage of 21 MeV protons is about 2.1 times the damage from 1 MeV neutrons (16). Numerical results on the Lorentz angles and shifts have been summarized in Table 1 and Table 2 and Fig. 6 and Fig. 7 before and after irradiation, respectively.

The temperature dependence of the Lorentz shift for holes is shown in Fig. 5. The Lorentz shift for both electrons and holes varies about 5 μm for a 300 μm thick sensor at 100 V in a 4 T magnetic field if the temperature is varied

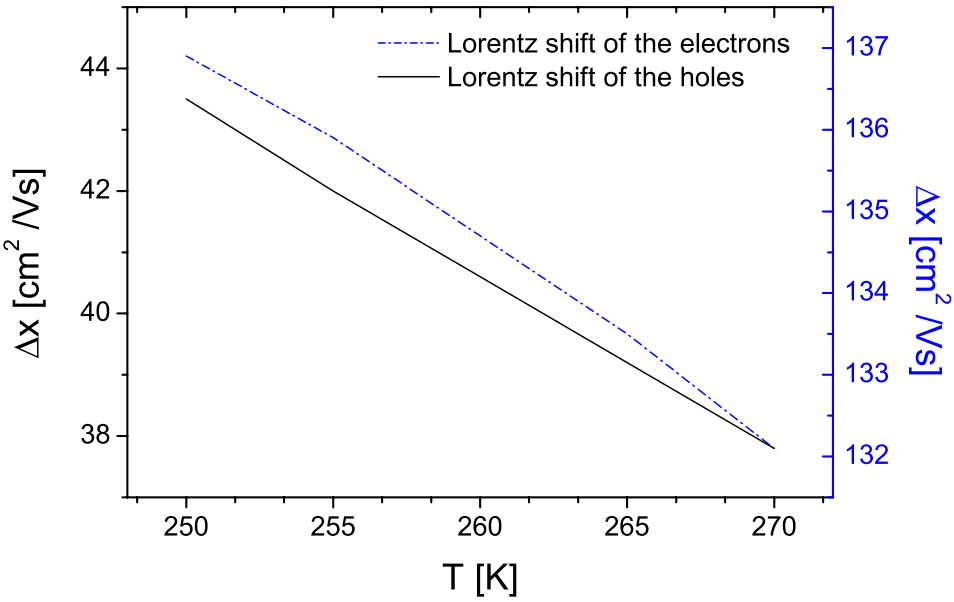

Fig. 5. *The Lorentz shift Δx for holes (lower curve) and electrons (top curve) generated at the surface simulated for a 300 µm thick sensor in a 4 T magnetic field at the bias voltage U_{bias} of 100 V versus temperature.*

between 250 K and 270 K.

The Lorentz angle for holes is not strongly depending on irradiation as shown in Fig. 6, while for electrons there is a clear dependence on the irradiation dose as shown in Fig. 7 and Table 2. The simulation of the Lorentz angles is described in Section 4.

4 Algorithm for the Lorentz angle of the silicon strip detectors

4.1 Non-irradiated sensors

Algorithms for the Lorentz shift will first be discussed for non-irradiated sensors and then conclusions for irradiated detectors will be drawn.

For a better understanding of the drift in the sensor simulations were performed. The mobility $\mu(E)$ is proportional to the mobility at low electric field μ_{low} and its behaviour at high electric fields is described with the help of a

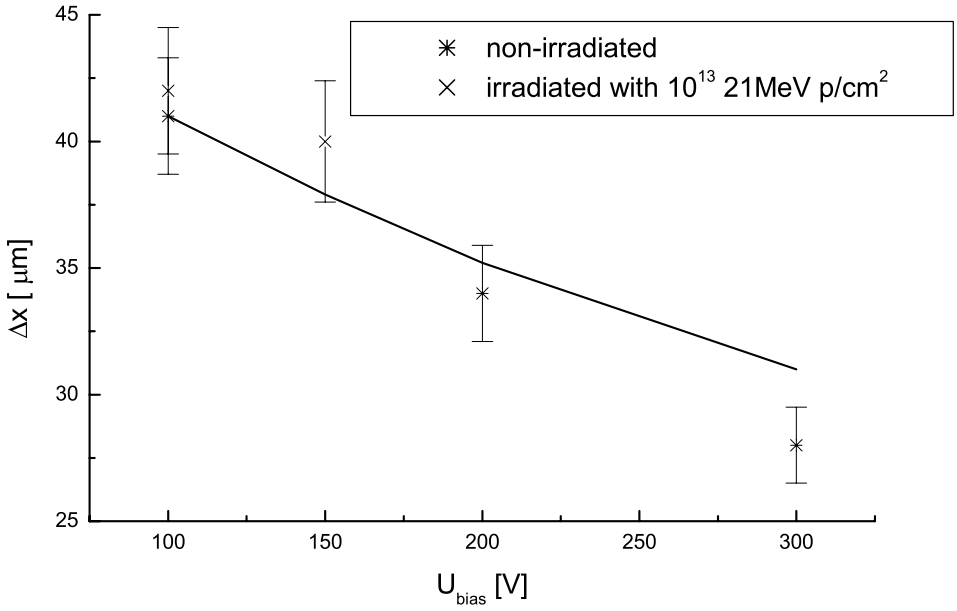

Fig. 6. *The Lorentz shift Δx for holes generated at the surface for a 300 μm thick sensor in a 4 T magnetic field versus bias voltage U_{bias}. The bars are systematic errors. The temperature is 260 K. The line is the result of the simulation.*

Table 1
Lorentz shift Δx for holes generated at the surface for a 300 μm thick sensor in a 4 T magnetic field as function of bias voltage for a non-irradiated sensor and an irradiated sensor. The sensor was irradiated with 21 MeV protons up to a fluence of 10^{13} p/cm^2. The full depletion voltages are 40 V for the non-irradiated sensor, 100 V for the irradiated sensor. The Lorentz shift for the non-irradiated sensor was measured at 270 K and corrected to 260 K using Eqs. 1, 3, 4.

non-irradiated					irradiated with 10^{13} 21 MeV p/cm^2			
U_{bias} in V	Δx in μm (270 K)	Δx in μm (260 K)	Θ_{meas} (270 K)	Θ_{sim} (270 K)	U_{bias} in V	Δx in μm (260 K)	Θ_{meas} (260 K)	Θ_{sim} (260 K)
100	38	41	7.2°	7.2°	100	42	8.0°	7.8°
200	31	34	5.9°	6.1°	150	40	7.6°	7.2°
300	25	28	4.8°	5.3°				

saturation velocity v_{sat} (3):

$$\mu(E) = \frac{\mu_{\mathrm{low}}}{(1 + (\frac{\mu_{\mathrm{low}} E}{v_{\mathrm{sat}}})^{\beta})^{\frac{1}{\beta}}} \tag{3}$$

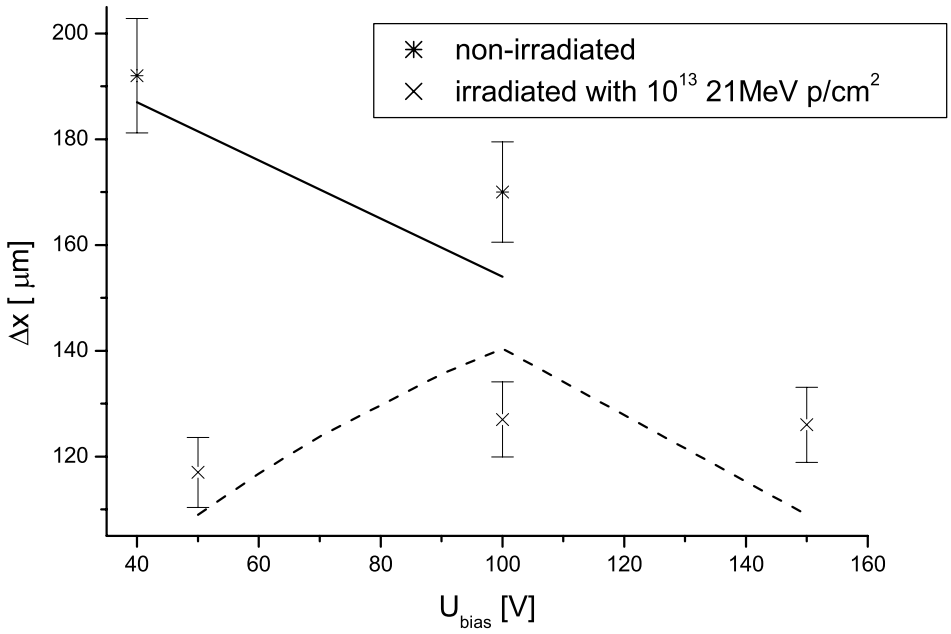

Fig. 7. *The Lorentz shift Δx for electrons generated at the surface for a 300 μm thick sensor in a 4 T magnetic field versus bias voltage U_{bias}. The bars are systematic errors. The temperature is 280 K. The lines are the results of the simulation.*

Table 2
Lorentz shift Δx for electrons generated at the surface for a 300 μm thick sensor in a 4 T magnetic field as function of bias voltage for a non-irradiated sensor and an irradiated sensor. The sensor was irradiated with 21 MeV protons up to a fluence of 10^{13} p/cm^2. The full depletion voltages are 40 V for the non-irradiated sensor, 100 V for the irradiated sensor. Θ_{sim} was obtained from the algorithm developed in Section 4.

non-irradiated				irradiated with 10^{13} 21 MeV p/cm^2			
U_{bias} in V	Δx in μm (280 K)	Θ_{meas} (280 K)	Θ_{sim} (280 K)	U_{bias} in V	Δx in μm (280 K)	Θ_{meas} (280 K)	Θ_{sim} (280 K)
40	192	33°	32°	50	117	21°	20°
100	170	30°	27°	100	127	23°	25°
				150	126	23°	22°

For holes the values are:

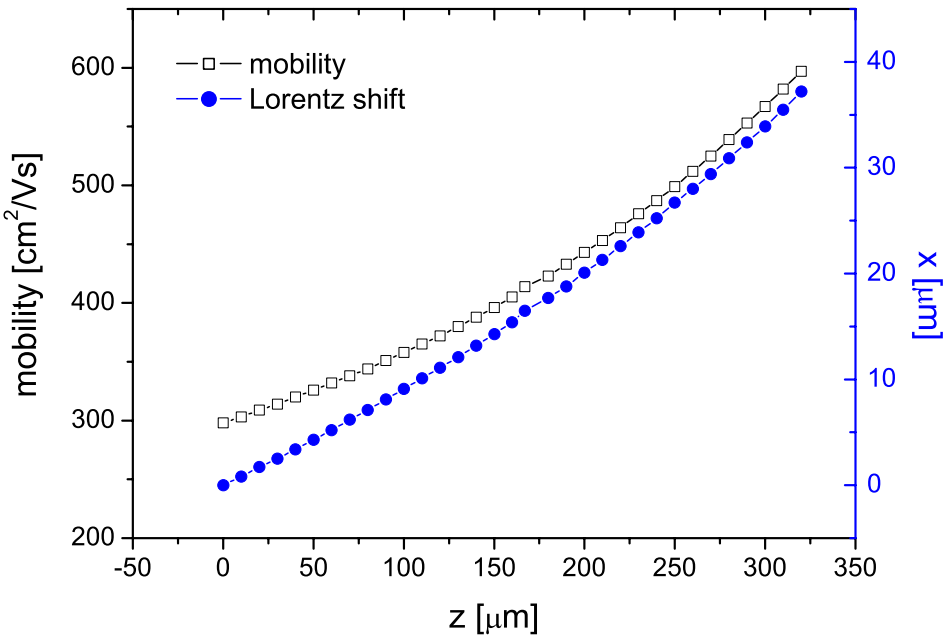

Fig. 8. *Simulated mean trajectory and mobility of holes at a full depletion voltage of 280 V and a bias voltage of 350V at a temperature of 263 K in a 4 T magnetic field. The thickness is 320 µm. The total Lorentz shift is 37 µm, the total shift calculated with a mean electric field is 36 µm.*

$$\mu_{\text{low}} = 470.5\frac{cm^2}{Vs} \cdot \left(\frac{T}{300}\right)^{-2.5}$$
$$\beta = 1.213 \cdot \left(\frac{T}{300}\right)^{0.17}$$
$$v_{\text{sat}} = 8.37 \cdot 10^6 cm/s \cdot \left(\frac{T}{300}\right)^{0.52}$$

For electrons the values are:

$$\mu_{\text{low}} = 1417\frac{cm^2}{Vs} \cdot \left(\frac{T}{300}\right)^{-2.2}$$
$$\beta = 1.109 \cdot \left(\frac{T}{300}\right)^{0.66}$$
$$v_{\text{sat}} = 1.07 \cdot 10^7 cm/s \cdot \left(\frac{T}{300}\right)^{0.87}$$

However the mobility is only slightly changing for bias voltages between full depletion and twice overdepletion. This leads to almost linear trajectories of the charge carriers, as shown in Fig. 8.

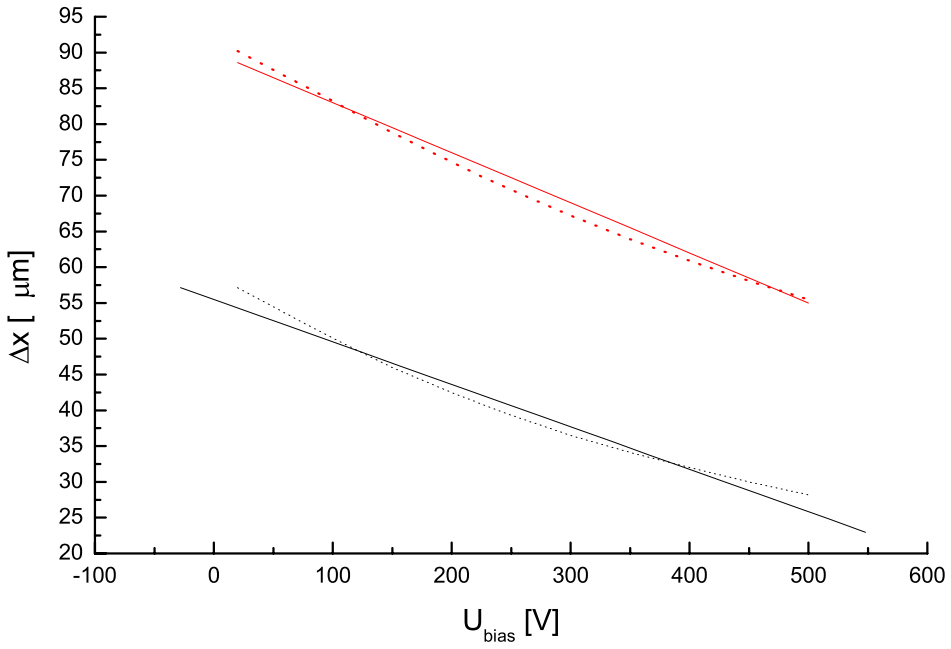

Fig. 9. *The Lorentz shift for holes generated at the surface Δx simulated for a 320 μm thick sensor (lower lines) and a 500 μm thick sensor (upper lines) in a 4 T magnetic field by Eqs. 1, 3 and 4. The dashed lines represent the linear approximation.*

Therefore a mean electric field E_{mean} is chosen, which depends only on the applied bias voltage U_{bias}:

$$E_{\text{mean}} = \frac{E(x=0) + E(x=d)}{2} = \frac{U_{\text{bias}}}{d} \tag{4}$$

For the now known average mobility, the Lorentz shift can be calculated from Eq. 1. Table 1 shows that the simulations match the measurement quite well.

Fig. 9 shows the simulated Lorentz shift as a function of the voltage for a 320 and 500 μm thick detector. The dependence of the Lorentz shift on the bias voltage is quite linear for fully depleted sensors.

Instead of calculating the Lorentz shift for holes generated at the surface from the mobility one can use the approximate linearity between bias voltage and Lorentz shift:

$$\Delta x = A - B \cdot U_{\text{bias}} \tag{5}$$

For a 320 μm thick sensor at 263 K in a 4 T magnetic field $A = 90\,\mu$m and $B = 0.07\,\mu$m/V. For a 500 μm thick sensor $A = 55\,\mu$m and $B = 0.06\,\mu$m/V.

There are three main parameters, which change after irradiation: the mobility, the electric field and the depletion voltage. As long as the sensor is fully depleted Eqs. 1, 3 and 4 can be used to calculate the Lorentz shift. The precise knowledge of the depletion voltage is not needed. So only the dependence of the mobility and the electric field on the radiation dose have to be discussed.

The dependence of the mobility on the irradiation dose is still controversial. In (17) no significant changes were observed in the transport properties of both electrons and holes up to $0.5{\cdot}10^{14}$ 1 MeV n/cm^2 and a prediction is made that a fluence of at least about 10^{15} 1 MeV n/cm^2 is necessary to affect carrier drift mobilities significantly. In (18) the mobility for both carrier types in irradiated sensors agree with those for the non-irradiated sensor within the errors for fluences up to $2{\cdot}10^{14}$ 1 MeV n/cm^2. In contrast a change of mobility after irradiation for holes and electrons was observed in (19).

- The mobility μ_{low} of holes changes slightly from 470 cm^2/Vs to about 460 cm^2/Vs after irradiation to a fluence of 10^{13} 1 MeV n/cm^2. Above this fluence the mobility does not change any more. The change of mobility corresponds to a change in the Lorentz shift of a few percent.

- The mobility μ_{low} of the electrons changes more significantly from 1417 cm^2/Vs to 1000 cm^2/Vs. The reduction of the mobility is so strong that one has to take this into account when computing the Lorentz shift.

This agrees with the measurements of Lorentz shift for electrons done in Karlsruhe. As demonstrated in Table 3 the data of the irradiated sensor can be well explained with the help of a reduced mobility μ_{low}.

In an irradiated sensors the so-called double junction effect arises. This effect has been observed (for example (21) and (22)) and modelled for a specific sensor using data from TCT (Transient Current Technique) measurements (20). A trend can be observed that with higher bias voltages the double junction effect is less pronounced. At bias voltages, which are equal or higher than the depletion voltage, the double junction effect is negligible for this sensor. As the CMS strip sensors are biased well above the depletion voltage, the double junction effect should be small.

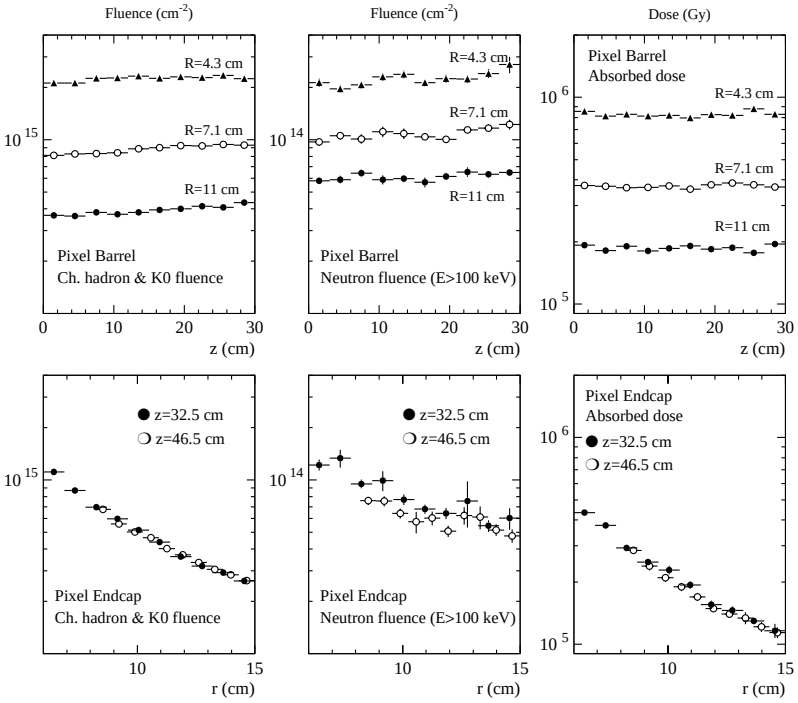

Fig. 10. *Energy-integrated charged hadron and neutron fluences and absorbed dose in the pixel detector. All values are for an integrated luminosity of 5·10^5 pb^{-1}. (5)*

5 Outlook: algorithm for the Lorentz angle of the pixel detector

The silicon pixel detector is situated 4.3 cm to 11 cm from the beam pipe. This results in a fluence up to about $2{\cdot}10^{15}$ 1 MeV n/cm^2 for an integrated luminosity of $5{\cdot}10^5$ pb^{-1}, which the pixel sensors have to stand. The distribution of the fluences over the silicon pixel detector is shown in Fig. 10 (5).

The design phase of the pixel detector is still going on, so some design parameters are not yet final. The thickness of the sensors will presumably be 250 μm. A maximum bias voltage of about 300 V is foreseen. For the final depletion depth after several years of operation, the resistivity of the initial n-material is not important, since type-inversion will occur very early in the experiment. So the depletion voltage is not yet known.

Fig. 11 shows that the full depletion voltage after a fluence of $3.6{\cdot}10^{14}$ pions/cm^2 of 300 MeV/c is about 500 V and increases to 1500 V after a fluence of $9{\cdot}10^{14}$ pions/cm^2 of 300 MeV/c (5). So the sensors cannot be fully depleted after exposure to these fluences. This influences the Lorentz shift, because the drift length of the electrons is shortened and therefore the Lorentz shift will be reduced (Fig. 12).

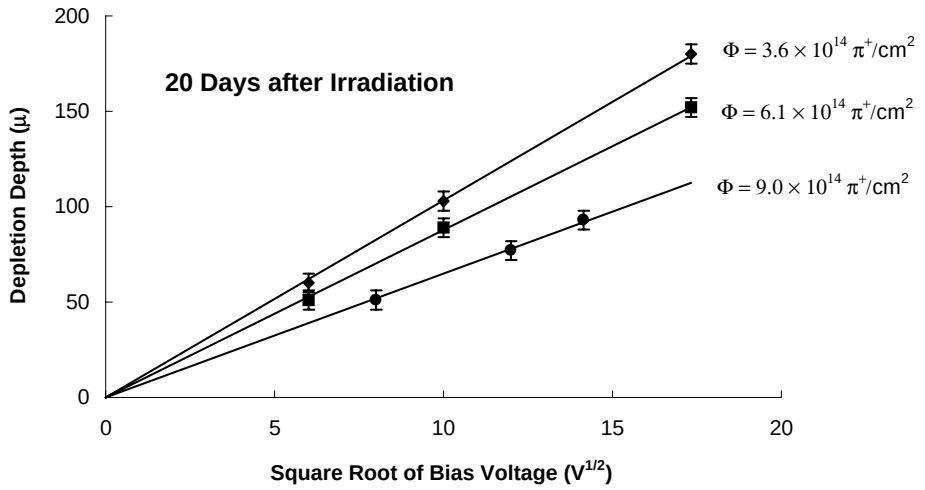

Fig. 11. *Depletion depth versus bias voltage for prototype pixel sensors. (5)*

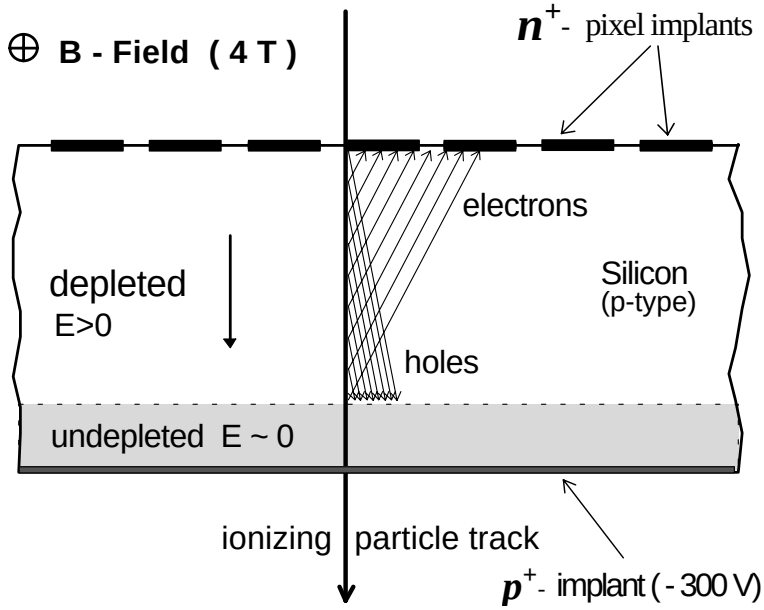

Fig. 12. *After type inversion the sensor depletes from the n-pixel side. With increasing radiation dose the sensor cannot be fully depleted and the total Lorentz shift is reduced. (5)*

The electric field in the pixel sensor changes much more than in the strip sensor since they are not fully depleted after irradiation. So the mobility of the electrons is not constant anymore as can be seen in Fig. 13. One has to divide the sensor into about five zones and then compute the shifts in each zone at an average electric field. The electric field is generally depending on the z-position, the bias voltage, the full depletion voltage U_{depl} and the thickness

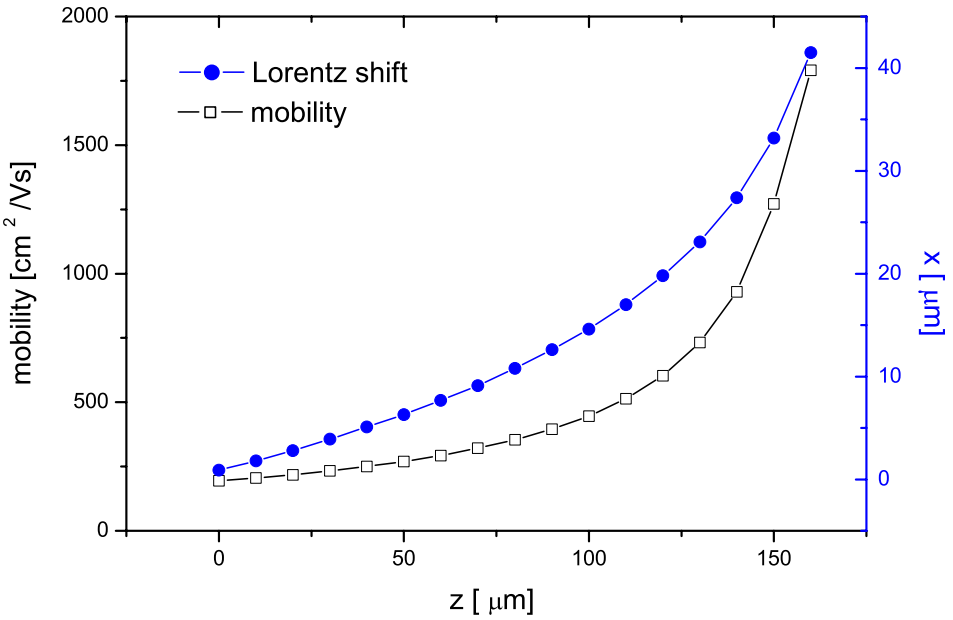

Fig. 13. *Simulated mean trajectory and mobility of electrons at a full depletion voltage of 1100 V and a bias voltage of 300 V at 263 K change strongly in the depleted zone of the sensor.*

of the sensor:

$$E(z) = \frac{U_{\text{bias}} - U_{\text{depl}}}{d} + \frac{2 \cdot U_{\text{depl}}}{d} \cdot \left(1 - \frac{z}{d}\right) \tag{6}$$

As pointed out in Subsection 4.2 the mobility of the electrons is likely to be dependent on the irradiation dose.

Table 3

The Lorentz shift Δx for electrons generated at the surface for a 300 µm thick sensor in a 4 T magnetic field at 280 K as function of bias voltage. The sensor was irradiated with 21 MeV protons up to a fluence of 10^{13} cm^2. The full depletion voltage is 100 V. Θ_{sim} with the reduced mobility fits the data Θ_{meas} better.

U_{bias} in V	Δx in μm	Θ_{meas}	Θ_{sim} $\mu_{\text{low}} = 1417\,\text{cm}^2/\text{Vs}$ at 300 K	Θ_{sim} $\mu_{\text{low}} = 1100\,\text{cm}^2/\text{Vs}$ at 300 K
50	117	21°	24°	20°
100	127	23°	29°	25°
150	126	23°	25°	22°

Because the sensor cannot be fully depleted after irradiation, the double junc-

tion effect, which arises at high fluences, is qualitatively larger than for fully depleted sensors. This effect has to be studied in detail in future.

Our algorithm is compared with measurements for the ATLAS pixel sensor reported in (13). The ATLAS pixel sensors are 280 μm thick and have a full depletion voltage before irradiation of about 150 V. The magnetic field during the measurements has been 1.4 T. The temperature was 300 K for the non-irradiated sensors and 263 K for the irradiated sensors. The measured values are compared to the simulated values in Table 4.

The algorithm divides the z-axis of the sensor into five parts. In each part the averaged mobility and corresponding Lorentz shift was calculated using the standard and reduced mobilities μ_{low} of Table 3. Comparing the simulations with the measurements one can see that the data can be fitted better with lower mobilities. So it has been shown that the proposed algorithm works for the pixel detectors.

Table 4
The Lorentz shift Δx for electrons for a 280 μm thick sensor in a 1.4 T magnetic field. The full depletion voltage before irradiation is 150 V. The measured data are taken from (13). The algorithm used for the simulation divides the sensor into five parts, in which the mean electric field and the corresponding the Lorentz shift are calculated. The averaged Lorentz angle is defined to be the arc tangent of the total Lorentz shift divided by the depletion depth. Θ_{sim} with the reduced mobility fits the data Θ_{meas} better.

Fluence n/cm^2	U_{bias} in V	Depl. depth in μm	Θ_{meas}	Θ_{sim} $\mu_{\mathrm{low}} = 1417\,\mathrm{cm}^2/\mathrm{Vs}$ at 300 K	Θ_{sim} $\mu_{\mathrm{low}} = 1100\,\mathrm{cm}^2/\mathrm{Vs}$ at 300 K
0	150	283	9.0°	8.4°	
$5{\cdot}10^{14}$	150	123	5.9°	6.7°	5.7°
$5{\cdot}10^{14}$	600	261	2.6°	4.4°	3.9°
10^{15}	600	189	3.1°	3.8°	3.5°
10^{15}	600	217	2.7°	3.2°	3.0°

6 Summary

The Lorentz angle is determined by electric and magnetic fields and can be modelled by Eqs. 1 and 3. Because of the different mobilities of holes and electrons, the Lorentz shift for electrons is about three times larger than for holes. The mobilities of the charge carriers saturate at high electric fields. The

mobility at low electric fields μ_{low} is decreased by irradiation more significantly for electrons than for holes. So for the electron mobility μ_{low} has to be changed after irradiation, but for holes the mobility can be kept.

The CMS pixel sensors collect electrons at the segmented side of the sensor, the CMS strip sensors collect holes. For the CMS strip sensor one can approximately use a mean electric field (Eq. 4). Therefore only the effects of a variation of bias voltages needs to be modelled.

For the CMS pixel sensor the electric field changes strongly inside the sensor, so the mobility has to be calculated for different points. In addition the mobility μ_{low} changes as a function of irradiation.

The simulated data have been compared with measured values from HERA-B test structures and the ATLAS pixel sensor. It has been shown that the algorithms developed in this work properly describe the effect of the Lorentz shift.

Acknowledgements

This work was done within the framework of the RD39 Collaboration (23). We thank Iris Abt for supplying us with double sided mini-strip detectors and Vitaliano Ciulli for discussing the CMS software.

References

[1] W. de Boer et al., Lorentz angle measurements in irradiated silicon detectors between 77K and 300K, *NIM A***461** (2001), 200–203.
[2] R.A. Smith, Semiconductors, *Cambridge Univ. Press*, 1968.
[3] C.Canali et al., Electron and hole drift velocity measurements in silicon and their empirical relation to electric field and temperature, *IEEE Trans. on Electron Devices*, Vol.**ED-22**, 1045–47, 1975.
[4] *CERN/LHCC 2000-16(2000)*, The CMS Collaboration, Addendum to the CMS Tracker TDR.
[5] *CERN/LHCC 98-6(1998)*, The CMS Collaboration, The Tracker Project Technical Design Report.
[6] *Pixel CMSIN1998/3*, R. Kaufmann and B. Henrich, Charge Drift in Silicon, 1998.
[7] E. Migliore, http://cmsdoc.cern.ch/Tracker/managment/Agenda_GTM/-Agenda_0101.html, 2001.
[8] E. Focardi et al., The CMS silicon tracker, *NIM A* **453**(2000), 121–125.

[9] F. Röderer, Messung von Lorentz-Winkeln in Silizium-Detektoren, Diplomarbeit, Univ. of Karlsruhe, IEKP–KA/98–24 (in german only).
[10] S. Heising, Silicon detectors for high energy physics experiments at low temperatures and high magnetic fields, Ph. D. thesis. Univ. of Karlsruhe, IEKP–KA/99–26 (in german only).
[11] F. Hauler, Lorentzwinkelmessungen an bestrahlten Silizium-Streifendetektoren im Temperaturbereich T=77-300K, Diplomarbeit, Univ. of Karlsruhe, IEKP–KA/2000–12 (in german only).
[12] E. Belau et al., Charge Collection in Silicon Strip Detectors, *NIM A* **214** (1983) 253.
[13] M. Aleppo, A measurement of Lorentz angle of radiation-hard pixel sensors, *NIM A* **465**(2001), 108–111.
[14] F. Hornung, A. Rimikes, Th. Schneider, High Magnetic Field facilities and Projects at the Forschungszentrum Karlsruhe, Internal Note, 1999.
[15] RD48 collaboration, http://rd48.web.cern.ch, *ROSE/TN/2000-03* .
[16] M. Huhtinen, Simulation of non-ionising energy loss and defect formation in silicon, *RD48 Technical Note 2001-02*, Cern(2001), submitted to NIM B.
[17] V. Eremin et al., Carrier drift mobility study in neutron irradiated high purity silicon, *NIM A* **362**(1995), 338–343.
[18] T.J. Brodbeck et al., Carrier Mobilities in Irradiated Silicon, *ROSE/TN/2000-09*.
[19] C. Leroy et al., Charge transport in non-irradiated and irradiated silicon detectors, *NIM A*(1999), 90–102.
[20] D. Menichelli et al., Modelling of the observed double-junction effect, *NIM A* **426**(1999), 135–139.
[21] L.J. Beattie et al., The electric field in irradiated silicon detectors, NIM A 418(1998), 314–321.
[22] G. Casse et al., Study of evolution of active volume in irradiated silicon detectors, *NIM A*(1999), 140–146.
[23] RD39 Collaboration, *NIM A* **440** (2000) 5-16 and http://rd39.web.cern.ch, RD39 Status Report CERN/LHCC 2000-010, 06-Jan-2000.
[24] V. Chabaud, Parameterizing detector specific effects for the Barrel of the DELPHI Silicon Tracker, *DELPHI 98-161 MVX 25* , 1998.
[25] L. Jones, Premux128 Specification, version 2.3, Rutherford Internal Note, 1995.
[26] Landolt-Börnstein, *Numerical Data and Functional Relationships in Science and Technology*, Group III, Vol. **17a**, Springer Verlag, Berlin, 1982.
[27] Technology Modelling Associates, Inc.: Davinci, Version 4.1, July 1998.